

The Effect of Interlayer Anion Grafting on Water Oxidation Electrocatalysis: A Comparative Study of Ni- and Co-Based Brucite-Type Layered Hydroxides, Layered Double Hydroxides and Hydroxynitrate Salts

A. V. Radha⁺,^[a] Sebastian Weiß⁺,^[a, b] Ignacio Sanjuán⁺,^[c] Michael Ertl,^[a] Corina Andronescu,^{*,[c]} and Josef Breu^{*,[a, b]}

Abstract: The urge for carbon-neutral green energy conversion and storage technologies has invoked the resurgence of interest in applying brucite-type materials as low-cost oxygen evolution reaction (OER) electrocatalysts in basic media. Transition metal layered hydroxides belonging to the brucite-type structure family have been shown to display remarkable electrochemical activity. Recent studies on the earth-abundant Fe³⁺ containing mössbauerite and Fe³⁺ rich Co–Fe layered oxyhydroxide carbonates have suggested that grafted interlayer anions might play a key role in OER catalysis. To probe the effect of such interlayer anion grafting in brucite-like layered hydroxides, we report here a systematic study on the electrocatalytic performance of three distinct Ni and Co

brucite-type layered structures, namely, (i) brucite-type M(OH)₂ without any interlayer anions, (ii) LDHs with free interlayer anions, and (iii) hydroxynitrate salts with grafted interlayer anions. The electrochemical results indeed show that grafting has an evident impact on the electronic structure and the observed OER activity. Ni- and Co-hydroxynitrate salts with grafted anions display notably earlier formations of the electrocatalytically active species. Particularly Co-hydroxynitrate salts exhibit lower overpotentials at 10 mA cm⁻² ($\eta = 0.34$ V) and medium current densities of 100 mA cm⁻² ($\eta = 0.40$ V) compared to the corresponding brucite-type hydroxides and LDH materials.

Introduction

The idea of storing excess energy from intermittent renewable solar and wind sources as an H₂ fuel is gaining traction as an efficient way to deliver a steady supply of renewable energy.^[1] Although the water-splitting reaction in an electrolyzer is expected to occur when an applied potential (E) reaches the

thermodynamic equilibrium potential ($E_{\text{eq}} = 1.23$ V), in practice, electrocatalysts need to be employed to reduce the overpotential ($\eta = E - E_{\text{eq}}$) and to lower the energy loss related to the kinetic barriers for hydrogen and oxygen evolution reactions.^[2] The main source for the observed overpotential is the oxygen evolution reaction (OER). It is a complex process as it requires a four-electron transfer to produce molecular oxygen at the anode. The current benchmark OER catalysts are noble-metal-based IrO₂ and RuO₂, which are expensive due to global scarcities of their mineral resources and are known to have long-term stability issues in alkaline media.^[3]

The initial OER studies dating back to the 1980s focused on Ni-, Co- and Fe-based hydroxides and (oxy)hydroxides as possible water oxidation catalysts in basic media.^[4] These studies were prompted by the observation of detrimental oxygen gas evolution at the positive electrode in nickel-cadmium (NiCd) and nickel-metal hydride (NiMH) rechargeable batteries. The last decade saw the resurgence of Ni-, Co-, and Fe-based, brucite-type layered materials as OER catalysts, thanks to several coinciding efforts to develop thin films of transition metal oxide, hydroxides, oxyhydroxide, and Ni-borate.^[5] Interestingly, these studies observed the in situ oxidation of layered hydroxide and oxyhydroxide during electrocatalysis, such as the α -Ni(OH)₂/ γ -NiO(OH) couple as depicted in the Bode's diagram.^[6] Later, Song et al. reported NiFe layered double hydroxide (LDH) and oxyhydroxide as OER catalysts, outperforming the benchmark IrO₂ catalyst.^[7] This encouraged widespread research on OER activities of transition metal-based

[a] A. V. Radha,⁺ S. Weiß,⁺ M. Ertl, Prof. Dr. J. Breu
 Department of Chemistry
 University of Bayreuth
 Universitätsstr. 30, 95447 Bayreuth (Germany)
 E-mail: josef.breu@uni-bayreuth.de

[b] S. Weiß,⁺ Prof. Dr. J. Breu
 Bavarian Center for Battery Technology (BayBatt)
 University of Bayreuth
 Universitätsstr. 30, 95447 Bayreuth (Germany)

[c] I. Sanjuán,⁺ Prof. Dr. C. Andronescu
 Technical Technology III and Center for Nanointegration (CENIDE)
 University Duisburg-Essen
 Carl-Benz-Str. 199, 47057 Duisburg (Germany)
 E-mail: corina.andronescu@uni-due.de

[⁺] These authors contributed equally to this work.

Supporting information for this article is available on the WWW under <https://doi.org/10.1002/chem.202100452>

Part of a Special Issue on Contemporary Challenges in Catalysis.

© 2021 The Authors. Chemistry - A European Journal published by Wiley-VCH GmbH. This is an open access article under the terms of the Creative Commons Attribution Non-Commercial License, which permits use, distribution and reproduction in any medium, provided the original work is properly cited and is not used for commercial purposes.

LDHs with various combinations of cations, exfoliated and electrodeposited ultrathin LDH sheets, as well as numerous graphite composites of LDHs.^[8]

Recently, our research group introduced two OER active materials, the earth-abundant Fe³⁺ containing mössbauerite,^[9] and Fe³⁺ rich Co–Fe layered (oxy)hydroxides.^[10] Later, a detailed structural analysis of mössbauerite by combining powder X-ray diffraction fitting with the DFT computed structural models revealed a randomly interstratified disordered structure with the interlayer carbonate partially grafted to the brucite layers.^[11] In line with this, previously, Hunter et al.^[12] identified some of the interlayer nitrite ions to be directly bound to Fe located at the edge of the brucite-type layer.

To the best of our knowledge, the effect of grafting anions to the brucite-type layers on the electrocatalytic performance has not been studied systematically. For selected transition metal cations such as Co and Ni, brucite-type materials, grafted hydroxy salts, and intercalated LDHs are accessible (Figure 1) and hence allowing for an investigation on the influence of grafting on their electrocatalytic performances.

Results and Discussion

Hydroxides of divalent first-row transition metal cations such as Ni²⁺, Co²⁺, Fe²⁺, Mn²⁺, Cu²⁺, and Zn²⁺ with ionic radii in the range of 0.60 to 0.75 Å crystallize in the brucite structure (Figure 1a) with an interlayer distance of 4.6 Å.^[13] LDHs of general formula [M²⁺_{6-z}M³⁺_z(OH)₁₂]{CO₃·nH₂O} with z = 1.2 to 2, are formed upon partial replacement of divalent with trivalent cations, which results in positive hydroxide layers that are charge compensated by hydrated interlayer anions (Fig-

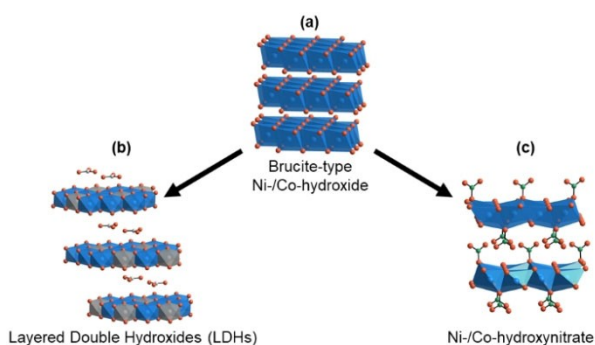


Figure 1. Schematic depiction of brucite-derived transition metal compounds investigated in this work.

ure 1b).^[14] Partial substitution of hydroxides with grafted anions leads to the third class of brucite-derived compounds known as metal hydroxy salts (Figure 1c) or hydroxide-rich basic salts, [M(OH)_{2-y}]{(Aⁿ⁻)_{y/n}·nH₂O} with distinct y values of 0.5, 0.67, and 1 and Aⁿ⁻ = NO₃⁻, Cl⁻, CO₃²⁻ or SO₄²⁻.^[15]

Unlike transition metal-based brucite M(OH)₂ and LDHs, basic hydroxy salts have received less attention as OER catalysts. For instance, Co-hydroxycarbonate on carbon paper ($\eta = 240$ mV at 10 mA cm⁻²)^[16] or Ni-foam ($\eta = 332$ mV at 10 mA cm⁻²)^[17] and CoMn-hydroxycarbonate on Ni-foam ($\eta = 294$ mV at 30 mA cm⁻²)^[18] have shown to catalyze OER at low overpotentials. However, these materials were either amorphous or poorly crystalline, with barely visible reflections in their PXRD patterns. The electrocatalytic studies on well-crystalline basic hydroxy salts are mostly limited to CoZn-hydroxy sulfate ($\eta = 370$ mV at 10 mA cm⁻² for Zn_{2.22}Co_{1.78}SO₄(OH)₆·0.5 H₂O) on a glassy carbon electrode.^[19] Ni-hydroxynitrate on Ni-foam exhibited the lowest overpotential ($\eta = 231$ mV at 50 mA cm⁻²)^[20] reported so far for hydroxy salts. Later it has, however, been shown that the Ni-foam itself contributes to the electrocatalytic activity.^[21]

The focus of this study is not reducing the overpotential to the minimum value. Instead, we want to gain insights into the effect of grafting on the overpotential by comparing the performance of three distinct Ni and Co brucite-derived layered structures, namely, (i) brucite M(OH)₂ without any interlayer anions, (ii) LDHs with free interlayer anions and (iii) hydroxynitrates with grafted interlayer anions.

For brucite structure, commercial reagent grade Ni(OH)₂ and Co(OH)₂ were used. The LDH structure requires trivalent cations. To avoid synergistic effects reported with Fe³⁺ in electrocatalysis,^[22] Al³⁺ is chosen as an electrochemically inert trivalent cation. Both NiAl-CO₃ and CoAl-CO₃ LDHs were obtained by urea hydrolysis. Ni and Co are known to exist as hydroxynitrate.^[23] Here, nitrate bonds or grafts directly to the metal cation, replacing hydroxide in the brucite layers (Figure 1c), leading to an interlayer distance of 6.9 Å, which is intermediate between brucite-type hydroxides (Figure 1a) and LDHs (Figure 1b).^[15]

Synthesis and Characterization of Compounds

The compositions of hydroxide samples, LDHs, and hydroxynitrates were determined by elemental analyses and were found to be within the expected range (Table 1). All X-ray powder diffraction traces could be fully indexed, indicating phase pure

Table 1. Summary of compositions and the cell parameters of Ni- and Co-based phases.

Sample	Composition	a (Å)	c (Å)	Polytype
Ni(OH) ₂	Ni(OH) ₂	3.127(5)	4.613(1)	1H
NiAl-CO ₃ LDH	Ni _{4.04} Al _{1.96} (OH) ₁₂ (CO ₃) _{0.98} ·2.5 H ₂ O	3.027(1)	22.57(1)	3R ₁
Ni-hydroxy-nitrate	Ni(OH) _{1.5} (NO ₃) _{0.5} ·0.12 H ₂ O	3.131(3)	6.869(1)	1H
Co(OH) ₂	Co(OH) ₂	3.183(0)	4.657(2)	1H
CoAl-CO ₃ -LDH	Co _{4.07} Al _{1.93} (OH) ₁₂ (CO ₃) _{0.97} ·3.2 H ₂ O	3.077(7)	22.83(2)	3R ₁
Co-hydroxy-nitrate	Co(OH) _{1.54} (NO ₃) _{0.46} ·0.05 H ₂ O	3.188(9)	20.79(8)	3R ₂

materials (Figures 2). The PXRD patterns of Ni(OH)₂ and Co(OH)₂ conform to a typical brucite structure (Figures 2a and d) with *P*-3*m*1 space group and refined cell parameters in close agreement with reported literature values (PDF: 14-117 (4.6 Å) and PDF: 30-443 (4.7 Å) for Ni(OH)₂ and Co(OH)₂, respectively; Table 1).

The PXRD patterns of NiAl-CO₃ and CoAl-CO₃ LDHs (Figure 2b and e) could be indexed with a three-layer rhombohedral cell with *R*-3*m* space group with interlayer distances of 7.52(3) Å and 7.61(0) Å for NiAl-CO₃ and CoAl-CO₃ LDHs, respectively, which is in perfect agreement with published values for carbonate intercalated LDHs (for instance 7.5 Å for NiAl-CO₃ (PDF: 015-0087)). In line with earlier studies, the presence of prominent mid-2θ reflections around 2.6 Å, 2.3 Å, and 1.9 Å in these PXRD patterns match with (012), (015), and (018) reflections supporting the 3*R*₁ polytype structure having a stacking sequence of *AC CB BA AC*.^[24]

As expected, for hydroxynitrates (Figure 2c and f), interlayer distances of 6.9 Å (Co-hydroxynitrate) and 7.0 Å (Ni-hydroxynitrate) were found to be intermediate between the values of the hydroxide and the LDH counterparts. This confirmed the presence of grafted nitrate anions. A nice integral series of (00*l*) reflections indicates a uniform interlayer distance with grafted anions being present in all interlayers. For both the Co- and Ni-hydroxynitrate salts (Figure 2c and f), (*hkl*) reflections with *l* ≠ 0 indicated ordered polytypes. For Ni-hydroxynitrate, the reflections observed at *d*-values of 6.9 Å, 3.5 Å, 2.7 Å, 2.5 Å, 2.1 Å, 1.7 Å, 1.6 Å, and 1.5 Å correspond to (001), (002), (100), (101), (102), (103), (110), and (111) reflections of the 1*H* polytype as

shown in earlier reported data (PDF: 022-0752).^[25] The non-systematic broadening of mid-2θ reflections between 30° to 50° (FWHM varying from 0.5° to 0.8° compared to 0.3° of basal ones), however, indicated a certain degree of stacking faults. As previously reported and contrary to Ni-hydroxynitrate, Co-hydroxynitrate crystallizes in the 3*R*₂ polytype with an *AC BA CB A* stacking sequence.^[26] The positions of the prominent mid-2θ reflections in Co-hydroxynitrate (Figure 2f) at 2.7 Å, 2.4 Å, and 2.0 Å are consistent with this earlier polytype assignment and correspond to (101), (104), and (107) reflections. Again, the non-systematic broadening of mid-2θ reflections (FWHM varying from 0.1° to 0.3° compared to 0.1° of basal ones) is due to the presence of stacking faults similar to its Ni analogue.

FTIR spectra of both, Ni(OH)₂ (Figure 3a) and Co(OH)₂ (Figure 3d), showed three absorptions bands in two different regions as typical for brucite structures: A sharp peak due to non-hydrogen bonded hydroxide groups around 3630 cm⁻¹, and two overlapping M–O vibration mode at ≈ 500 cm⁻¹.

FTIR spectra of NiAl-CO₃ (Figure 3b) and CoAl-CO₃ LDHs (Figure 3e) displayed peaks in three different regions due to the presence of interlayer anions and interlayer water molecules in addition to structural hydroxyl anions. The hydroxide stretching modes in LDHs appear to be broad and shifted to a lower region around ≈ 3400 cm⁻¹ due to hydrogen bonding with the interlayer water molecules. The corresponding bending mode showed up as a weak signal at 1600 cm⁻¹.^[27] A large mass difference between the transition metal Ni/Co and Al cations split the M–O–H bending modes into a doublet at 560 and 615 cm⁻¹. Additional peaks like a strong ν₃ band at 1350 cm⁻¹

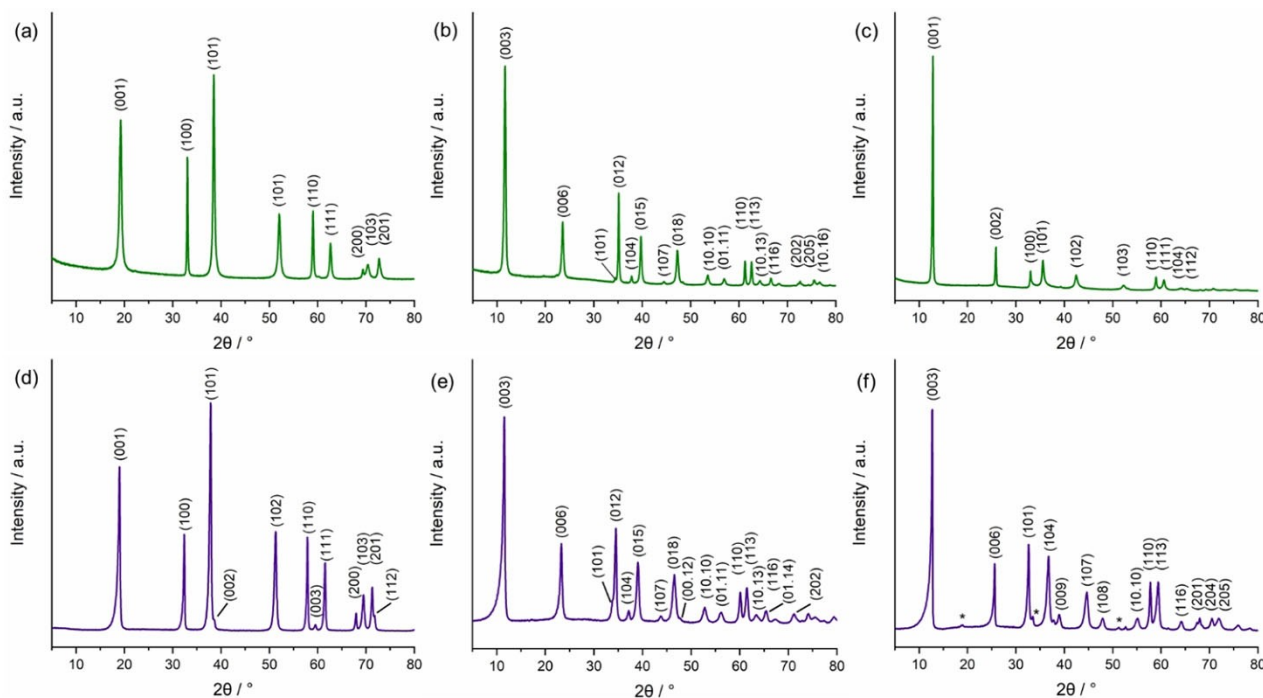


Figure 2. PXRD patterns of Ni-compounds (top): (a) Ni(OH)₂ without interlayer anions, (b) NiAl-CO₃ LDH, and (c) Ni-hydroxynitrate with grafted nitrate anion. PXRD patterns of Co-compounds (bottom): (d) Co(OH)₂ without interlayer anions, (e) CoAl-CO₃ LDH, and (f) Co-hydroxynitrate with grafted nitrate anion. A minor Co(OH)₂ impurity in (f) is marked with an asterisk.

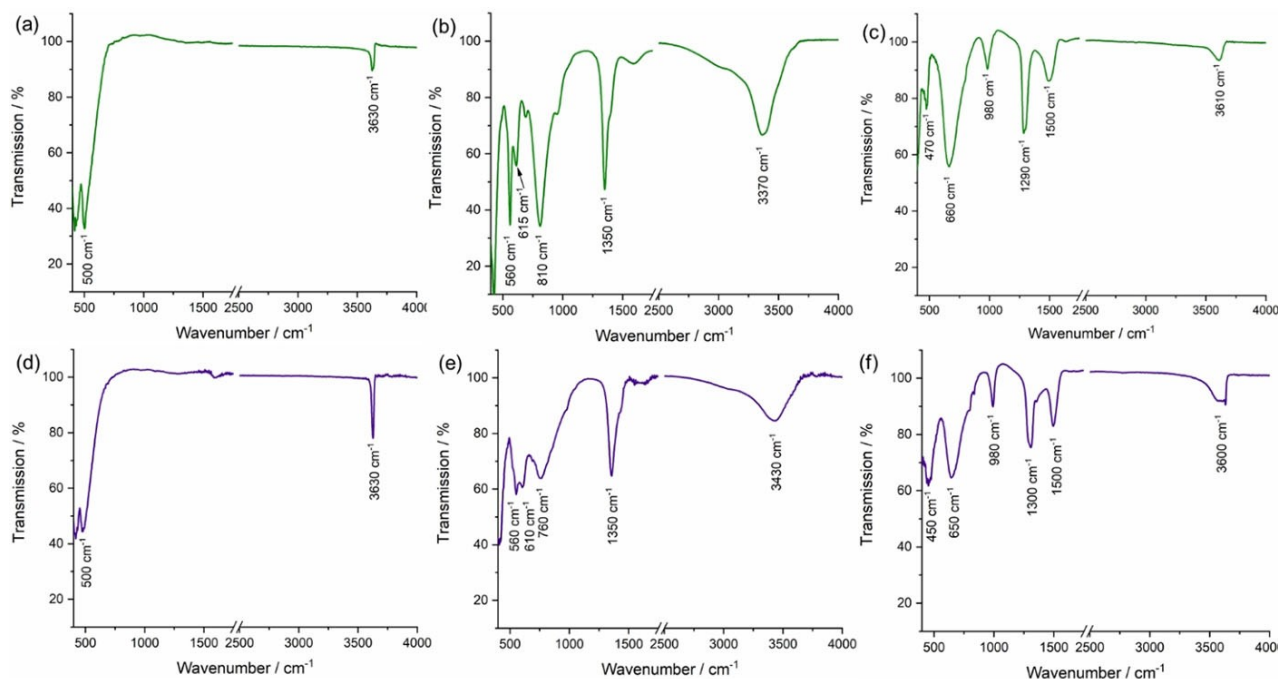


Figure 3. FTIR spectra of Ni-compounds (top): (a) Ni(OH)₂ without interlayer anions, (b) NiAl-CO₃ LDH, and (c) Ni-hydroxynitrate with grafted nitrate anion. FTIR spectra of Co-compounds (bottom): (d) Co(OH)₂ without interlayer anions, (e) CoAl-CO₃ LDH, and (f) Co-hydroxynitrate with grafted nitrate anion.

along with two weak signals due to ν_2 and ν_4 modes around 810 and 667 cm⁻¹ that overlap with the M–O lattice vibrations modes confirmed the presence of intercalated carbonate anion in D_{3h} symmetry in both LDHs.

The FTIR spectra of Ni- (Figure 3c) and Co-hydroxynitrate (Figure 3f) were distinctly different from the LDH spectra regarding both wavenumbers and the splitting of the bands. For instance, the band due to the hydrogen-bonded hydroxide group appeared as a broad peak around 3600 cm⁻¹ and M–O–OH and M–O lattice vibration modes at ca. 650 and ca. 450 cm⁻¹, respectively. A strikingly distinct part was the presence of three strong absorption bands at 1300 cm⁻¹, 1500 cm⁻¹, and 980 cm⁻¹, which could be assigned to ν_{1i} , ν_4 , and ν_3 , vibration modes of the nitrate anion with symmetry lowered to C_{2v} . The presence of two distinct ν_1 and ν_4 modes with a wavenumber difference of 200 cm⁻¹ indicated that one oxygen of nitrate is directly bound to the metal cation completing its octahedral coordination shell. This provides direct experimental evidence for the nitrate grafting in both Ni- and Co-hydroxynitrate.

As evidenced by the SEM micrographs (Figure 4), all compounds tend to form larger, intergrown aggregates of platy crystals as expected for layered structures. The corresponding BET surface areas are depicted in the micrographs and give a first hint regarding the accessible surface, solely based on morphological considerations. For Ni-based compounds, the NiAl-CO₃ LDH and Ni(OH)₂ feature the highest and the lowest surface area, respectively. Similarly, the CoAl-CO₃ LDH resembles the compound with the highest BET surface area, while the Co-hydroxynitrate features the lowest. Based on these structural

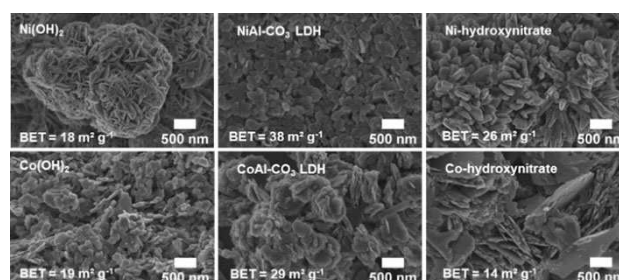


Figure 4. SEM micrographs of Ni- (top) and Co- (bottom) compounds: Ni(OH)₂ and Co(OH)₂ without interlayer anions (left), NiAl-CO₃ LDH and CoAl-CO₃ LDH (middle), and Ni-/Co-hydroxynitrate with grafted nitrate anion (right) with corresponding BET values.

considerations alone, the samples with the lowest accessible surface area are expected to perform the least active in OER catalysis.

However, as the active site for OER has been proposed to be located at the edges of the brucite layers rather than the planes, activity is expected to increase with the surface area and the contribution of the edges to it.^[28] Thus, platelets with small diameters and small aspect ratio (diameter/thickness) should be most advantageous. To determine the accessibility based on the electrochemically active surface area, double layer capacitance measurements are performed complementary to the electrocatalytic measurements in the following section.

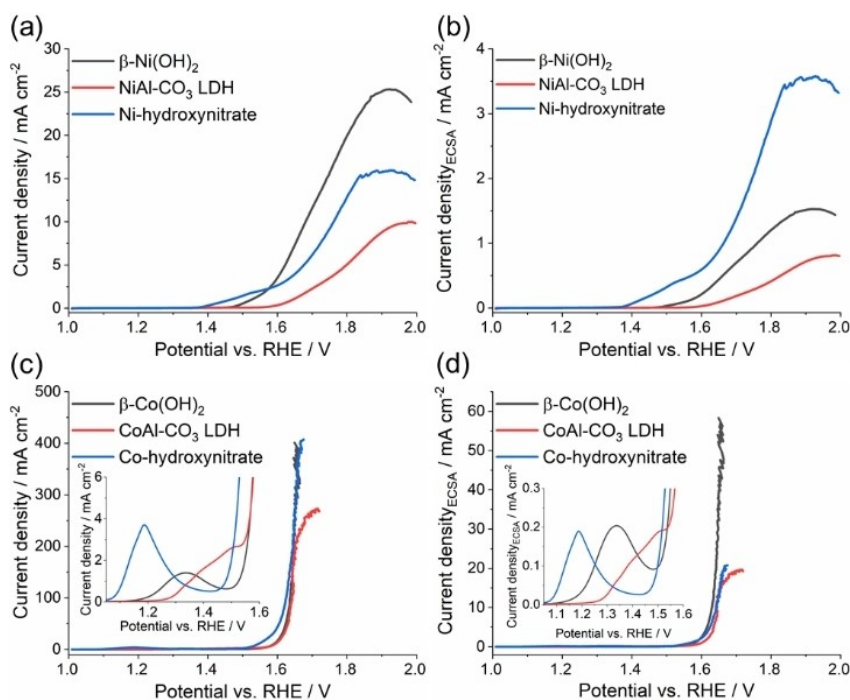


Figure 5. Linear sweep voltammograms of the Ni- (a and b) and Co-based compounds (c and d). LSVs were recorded with a scan rate of 5 mVs^{-1} , and RDE speed of 1600 rpm in O_2 saturated purified 1 M KOH solutions. In plots (a) and (c), the current density is calculated using the geometric area of the electrode. In contrast, in plots (b) and (d), the current density is calculated using the ECSA.

Sample	ECSA (cm^2)	Overpotential η (V) 10 mA cm^{-2}	Overpotential η (V) 10 mA cm^{-2} (ECSA)	Overpotential η (V) 100 mA cm^{-2}
Ni(OH)_2	1.88 ± 0.09	0.49 ± 0.03	–	–
$\text{NiAl-CO}_3\text{-LDH}$	1.39 ± 0.17	–	–	–
Ni-hydroxy-nitrate	0.51 ± 0.01	0.56 ± 0.03	–	–
Co(OH)_2	0.80 ± 0.02	0.358 ± 0.003	0.40 ± 0.01	0.414 ± 0.009
$\text{CoAl-CO}_3\text{-LDH}$	1.57 ± 0.03	0.366 ± 0.005	0.415 ± 0.001	0.416 ± 0.003
Co-hydroxy-nitrate	2.22 ± 0.10	0.34 ± 0.02	0.415 ± 0.002	0.401 ± 0.005

OER electrocatalysis of Ni and Co compounds

The OER electrocatalytic performance of the different brucite-type layered materials was analyzed using linear sweep voltammograms recorded in the OER potential window (Figure 5). The normalization of the recorded currents was done using both geometric area of the catalyst film, as well as its ECSA evaluated from the cyclic voltammograms recorded in the non-Faradaic region using different scan rates (Table 2). When normalized to the geometric area, significantly higher activity is observed for Co-based compounds, for which current densities up to hundreds of mA cm^{-2} are recorded with $\sim 400 \text{ mV}$ overpotential. At the same time, in the same potential window, just a few tenths of mA cm^{-2} are generated for the Ni-based materials (Figure 5, Table 2). This fact suggests the superior activity of Co-based compounds towards OER and is in line with the proposed activity trend for different transition-metal (oxy) hydroxides in alkaline media.^[29]

In the LSVs recorded using the Ni-based compounds (Figure 5a and b), different features are observed associated with the Ni^{2+} oxidation. In the case of $\beta\text{-Ni(OH)}_2$ and Ni-hydroxynitrate, the Ni^{2+} electro-oxidation to Ni^{3+} was observed as a pre-oxidation shoulder which appeared at potentials below OER. In the case of Ni-hydroxynitrate, Ni^{2+} electro-oxidation occurred at more cathodic potentials ($\sim 1.4 \text{ V}$ vs. RHE) than in the case of $\beta\text{-Ni(OH)}_2$ ($\sim 1.45 \text{ V}$ vs. RHE), while for NiAl- CO_3 LDH, no clear Ni^{2+} oxidation peak could be observed. This indicates that the grafted nitrate anions influence the oxidation of Ni^{2+} , allowing its conversion to the active Ni^{3+} OER electrocatalyst at more cathodic potentials already. Different activity trends were observed depending on the area used to normalize the recorded currents, the geometric or the ECSA one. While the normalization by the geometric area indicates $\beta\text{-Ni(OH)}_2$ as the most active, the normalization to the ECSA concludes that Ni-hydroxynitrate shows the highest catalytic activity of Ni-based electrocatalysts. Based on these findings, we conclude that

electrocatalytic centers in Ni-hydroxynitrate are the most active. Still, the overall performance suffers from the lower number of active sites accessible due to its morphology. The rotating ring disk electrode (RRDE) technique was used to confirm the O₂ formation on the Co- and Ni hydroxynitrates (Figure S1). The faradaic efficiencies (FE) of O₂ obtained using Ni-hydroxynitrate at +1.5 V vs. RHE was 91 ± 9% indicating that the recorded currents correspond mainly to the OER.

As observed for the Ni-hydroxynitrate, and also in the case of Co-hydroxynitrate, an oxidation peak associated with Co²⁺ oxidation^[30] was present at ~1.2 V. In comparison, for β-Co(OH)₂ and CoAl-CO₃ LDH, an oxidation process was observed at more anodic potentials with ~1.35 V and 1.4 V vs. RHE, respectively. This suggests that the presence of grafted nitrate anions is influencing the formation of the Co³⁺ species. Different activity trends were also observed for the Co-based compounds when comparing the potentials at which a current density of 10 mA cm⁻² was obtained, depending on the considered area. When the geometric area is used, Co-hydroxynitrate shows the highest activity reaching 10 mA cm⁻² at 0.34 V overpotential while β-Co(OH)₂ requires 0.36 V. At a higher current density of 100 mA cm⁻², the Co-hydroxynitrate still allows for a lower overpotential than the other materials under investigation. With an overpotential of 0.4 V, it performs better than the β-Co(OH)₂ (0.41 V) and the CoAl-CO₃ LDH (0.42 V). When the ECSA is considered, the Co-hydroxynitrate initially shows the earliest onset of OER. However, at a current density of 10 mA cm⁻² the recorded overpotential for β-Co(OH)₂ is 0.4 V while 10 mV more are needed for Co-hydroxynitrate and CoAl-CO₃ LDH. These differences are not as pronounced as in Ni-based materials, indicating that in the case of Co-based materials, nitrate grafting influences the oxidation of Co²⁺. Still, overall the OER electrocatalytic activity is not so strongly affected as in Ni-based compounds. Since higher current densities are recorded on Co hydroxynitrate compared with the Ni one, to quantify the formed O₂, we used a gas chromatograph coupled to a gas-tight electrochemical cell. In this case, the Co-hydroxynitrate catalyst was deposited on carbon paper, and the electrolysis was performed in galvanostatic mode. We started by applying 15 mA (3.75 mA cm⁻²), and we increased the current up to 200 mA (50 mA cm⁻²). The produced O₂ was quantified by gas chromatography, and FE values in the range 91-103 were calculated (Figure S3). For example, at 50 mA cm⁻², the calculated FE is 95 ± 1%.

In general, the performance of electrocatalysts must be interpreted in terms of oxidation state, electronic structure, and coordination state of the active metal sites.^[8b] *In-situ* studies of layered electrocatalysts have recognized the transition metal positions located at the edges and corners of the layers as more active OER sites.^[31] Here, synergistic effects based on metal cations in the second coordination sphere are regarded negligible as the catalytic activity of CoAl-CO₃ LDH ($\eta = 366$ mV at 10 mA cm⁻²) is comparable to NiCo-CO₃ and CoCo-CO₃ LDHs with overpotentials of 385 and 395 mV at 10 mA cm⁻².^[7] Thus, we assume that the effect of electrochemically inactive, structural Al can indeed be neglected.

Ni-hydroxynitrate showed the earliest formation of electrocatalytically active Ni³⁺ from all Ni-based compounds. Similarly, among all Co-based samples studied, Co-hydroxynitrate additionally featured the highest OER activity up to 407 mA cm⁻². This would indicate that the grafted anion of hydroxy salts triggers a larger separation of individual layers than the hydroxide compounds. Thus, it improves the accessibility of electrochemically active cation sites for OER catalysis at the edges, facilitating the OER reaction. Furthermore, the electronic structure and thus redox activity is modulated by the formal replacement of hydroxide by nitrate anions. According to the spectrochemical row,^[32] the electron-donating capability of hydroxide ions is expected to be higher than those of the nitrate-ions. Thus, a lower electron density is expected at the electrocatalytically active transition-metal centers for hydroxy salts compared to hydroxide or LDH compounds. Previous investigations on NiFe-LDHs have shown that charge delocalization and reduced electron density created by incorporating electron-withdrawing anions or cations can facilitate higher-valent electrophilic transition metal ion sites. These can promote the nucleophilic attack of hydroxyl and water molecules and thus improve the adsorption of the reaction intermediate during OER.^[33]

To further understand the potential of hydroxynitrates as OER electrocatalysts, their stability was evaluated by current-controlled electrolysis (Figure 6a). A constant current corresponding to 10 mA cm⁻² current density was applied for 2 h while continuously monitoring the potential. While Ni-hydroxynitrate shows an initial deactivation, followed by activation with time, a constant potential is recorded when using Co-hydroxynitrate (Figure 6b), indicating superior stability of the latter with time at these moderate electrolysis conditions. For the Co-hydroxynitrate catalyst, we analyzed every 15 minutes the concentration of the formed O₂ during the 2 h electrolysis. The calculated FEs indicate a stable electrolysis process in which O₂ is produced with FE close to 100% without significant variations over the course of the 2 h (Figure S4).

LSVs recorded for both materials before and after the stability test support the previous observation. While for Ni-hydroxynitrate, higher current densities are recorded after the prolonged electrolysis (Figure S7), in the case of Co-hydroxynitrate, a slight decay of the activity is observed, probably due to

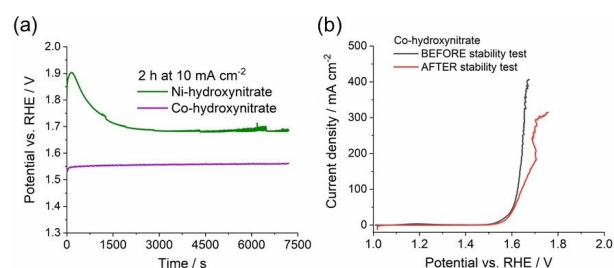


Figure 6. (a) Chronopotentiometric measurements performed in 1 M KOH at a current density corresponding to 10 mA cm⁻² for 2 h under 1600 rpm, using Co- and Ni-hydroxynitrate modified GC electrodes; (b) LSVs recorded for the Co-hydroxynitrate modified GC before and after the stability test.

decreased conductivity of the Co-hydroxynitrate as it can be observed from the LSV slope. Still, the Co-hydroxynitrate shows higher electrocatalytic activity compared with the Ni one. No significant changes can be noticed on the electrocatalysts film based on the SEM pictures taken before and after the stability measurement.

Post-electrolysis XRD analysis was performed for both the Ni-hydroxynitrate (Figure S8) and the Co-hydroxynitrate (Figure S9). Both XRD patterns show the presence of the initial catalyst with some side phases formed during the 2 h electrolysis. However, an unaltered basal spacing of the layered structures indicates that the interlayer space composition has not changed over the course of the experiment. For Ni-hydroxynitrate, some of the additional reflections can be assigned to the presence of $K_2Ni(CO_3)_2$ (PDF: 00-046-0783), K_2CO_3 (PDF: 00-011-0655), and NiO (PDF: 00-047-1049). Previous studies of this catalyst have also shown the alteration of the surface layer upon prolonged electrolysis.^[3,4] The newly formed phases can contribute to the fluctuations observed in the chronopotentiometric measurements. Besides this, possible catalyst dissolution occurring during the electrolysis process can change the catalyst film conductivity and generate a catalyst film with an overall higher electrocatalytic activity. In Co-hydroxynitrate, evidence for the presence of Co_3O_4 (PDF: 00-042-1467) and K_2CoO_2 (PDF: 00-049-1556) can be found. Post-electrolysis EDX measurements for Ni- and Co-hydroxynitrate indicate no detectable incorporation of secondary metal ions from the electrolyte (Figure S10, S11). Despite the fact that secondary phases formed during the 2 h electrolysis, no significant impact can be noticed in the overall performance of the Co-hydroxynitrate coated electrode.

Conclusion

Grafting of anions to brucite-type layered structures formally represents a substitution of hydroxides, for example, by nitrate. On the one hand, adjacent layers are separated to larger distances allowing for easier access to active sites at the edges. On the other hand, the nitrate ligand's basicity is smaller than the hydroxide ligand, and the electron density at the metal center is reduced. Both factors may contribute to the observed increased OER efficiency of hydroxy salts than simple hydroxides or LDH structures. While hydroxy salts are less flexible with respect to compositional variations than LDHs, doping, for instance, with Fe, will be feasible to some extent. During 2 h electrolysis performed at 10 mA cm^{-2} , both Co and Ni-hydroxynitrates form secondary phases, as often observed for transition metal-based OER electrocatalysts. Hydroxy salts show high versatility, being accessible for various anions like acetate, sulfate, carbonate, perchlorates, and halides. Based on previous experience with NiFe-LDHs, further performance improvement should be achievable this way. Hydroxy salts certainly deserve further attention in the electrocatalysis world.

Acknowledgements

The authors are grateful for financial support by the Deutsche Forschungsgemeinschaft (DFG) in the framework of the SFB 840. We thank Prof. Mirijam Zobel for the measurement time with her powder X-ray diffractometer as well as Anna-Maria Dietel for CHN analysis of the samples. We thank Lena Geiling and Marco Schwarzmann for SEM measurements and BayCEER for ICP-OES measurements. We thank Renee Timmins for English proofreading. S.W. acknowledges the support from the Elite Network of Bavaria and thanks the graduate school of the Bavarian Center for Battery Technology (BayBatt) for ongoing support. C.A. acknowledges the financial support by DFG in the framework of the CRC 247. Open access funding enabled and organized by Projekt DEAL.

Conflict of Interest

The authors declare no conflict of interest.

Keywords: electrochemistry · nickel/cobalt hydroxynitrate · nitrate grafting · oxygen evolution reaction · water splitting

- [1] a) H. L. Tuller, *Mater. Renew. Sustain. Energy* **2017**, *6*, 3; b) Z. Yan, J. L. Hitt, J. A. Turner, T. E. Mallouk, *Proc. Natl. Acad. Sci. USA* **2020**, *117*, 12558–12563.
- [2] R. L. Doyle, M. E. G. Lyons, *Photoelectrochemical Solar Fuel Production: From Basic Principles to Advanced Devices* (Eds.: S. Giménez, J. Bisquert), Springer International Publishing, Cham, **2016**, pp. 41–104.
- [3] a) S. Trasatti, *J. Electroanal. Chem.* **1980**, *111*, 125–131; b) Y. Lee, J. Suntivich, K. J. May, E. E. Perry, Y. Shao-Horn, *J. Phys. Chem. Lett.* **2012**, *3*, 399–404.
- [4] a) D. E. Hall, *J. Electrochem. Soc.* **1983**, *130*, 317; b) M. R. Gennerio de Chialvo, A. C. Chialvo, *Electrochim. Acta* **1988**, *33*, 825–830; c) D. A. Corrigan, *J. Electrochem. Soc.* **1987**, *134*, 377.
- [5] a) L. Trotochaud, J. K. Ranney, K. N. Williams, S. W. Boettcher, *J. Am. Chem. Soc.* **2012**, *134*, 17253–17261; b) D. K. Bediako, B. Lassalle-Kaiser, Y. Surendranath, J. Yano, V. K. Yachandra, D. G. Nocera, *J. Am. Chem. Soc.* **2012**, *134*, 6801–6809; c) R. L. Doyle, I. J. Godwin, M. P. Brandon, M. E. G. Lyons, *Phys. Chem. Chem. Phys.* **2013**, *15*, 13737–13783.
- [6] H. Bode, K. Dehmelt, J. Witte, *Electrochim. Acta* **1966**, *11*, 1079–1087.
- [7] F. Song, X. Hu, *Nat. Commun.* **2014**, *5*, 4477.
- [8] a) N.-T. Suen, S.-F. Hung, Q. Quan, N. Zhang, Y.-J. Xu, H. M. Chen, *Chem. Soc. Rev.* **2017**, *46*, 337–365; b) Y. Wang, D. Yan, S. El Hankari, Y. Zou, S. Wang, *Adv. Sci.* **2018**, *5*, 1800064.
- [9] M. Ertl, C. Andronesco, J. Moir, M. Zobel, F. E. Wagner, S. Barwe, G. Ozin, W. Schuhmann, J. Breu, *Chem. Eur. J.* **2018**, *24*, 9004–9008.
- [10] S. Weiß, M. Ertl, S. D. Varhade, A. V. Radha, W. Schuhmann, J. Breu, C. Andronesco, *Electrochim. Acta* **2020**, *350*, 136256.
- [11] P. Lyu, M. Ertl, C. J. Heard, L. Grajciar, A. V. Radha, T. Martin, J. Breu, P. Nachtigall, *J. Phys. Chem. C* **2019**, *123*, 25157–25165.
- [12] B. M. Hunter, W. Hieringer, J. R. Winkler, H. B. Gray, A. M. Müller, *Energy Environ. Sci.* **2016**, *9*, 1734–1743.
- [13] H. R. Oswald, R. Asper, *Preparation and Crystal Growth of Materials with Layered Structures* (Ed.: R. M. A. Lieth), Springer Netherlands, Dordrecht, **1977**, pp. 71–140.
- [14] H. F. W. Taylor, *Mineral. Mag.* **1973**, *39*, 377–389.
- [15] a) M. Rajamathi, G. S. Thomas, P. V. Kamath, *J. Chem. Sci.* **2001**, *113*, 671–680; b) S. P. Newman, W. Jones, *J. Solid State Chem.* **1999**, *148*, 26–40.
- [16] S. Zhang, B. Ni, H. Li, H. Lin, H. Zhu, H. Wang, X. Wang, *Chem. Commun.* **2017**, *53*, 8010–8013.
- [17] M. Xie, L. Yang, Y. Ji, Z. Wang, X. Ren, Z. Liu, A. M. Asiri, X. Xiong, X. Sun, *Nanoscale* **2017**, *9*, 16612–16615.

- [18] T. Tang, W.-J. Jiang, S. Niu, N. Liu, H. Luo, Y.-Y. Chen, S.-F. Jin, F. Gao, L.-J. Wan, J.-S. Hu, *J. Am. Chem. Soc.* **2017**, *139*, 8320–8328.
- [19] S. Dutta, C. Ray, Y. Negishi, T. Pal, *ACS Appl. Mater. Interfaces* **2017**, *9*, 8134–8141.
- [20] Y. Ma, J. Chu, Z. Li, D. Rakov, X. Han, Y. Du, B. Song, P. Xu, *Small* **2018**, *14*, 1803783.
- [21] X. Hu, X. Tian, Y.-W. Lin, Z. Wang, *RSC Adv.* **2019**, *9*, 31563–31571.
- [22] a) F. Yang, K. Sliozberg, I. Sinev, H. Antoni, A. Bähr, K. Ollegott, W. Xia, J. Masa, W. Grünert, B. R. Cuenya, W. Schuhmann, M. Muhler, *ChemSusChem* **2017**, *10*, 156–165; b) L. Trotochaud, S. L. Young, J. K. Ranney, S. W. Boettcher, *J. Am. Chem. Soc.* **2014**, *136*, 6744–6753.
- [23] M. Rajamathi, P. Vishnu Kamath, *J. Power Sources* **1998**, *70*, 118–121.
- [24] A. V. Radha, P. V. Kamath, C. Shivakumara, *Acta Crystallogr. Sect. B* **2007**, *63*, 243–250.
- [25] D. Louër, *J. Solid State Chem.* **1975**, *13*, 319–324.
- [26] a) T. N. Ramesh, *Inorg. Chem. Commun.* **2009**, *12*, 832–834; b) T. N. Ramesh, M. Rajamathi, P. Vishnu Kamath, *J. Solid State Chem.* **2006**, *179*, 2386–2393.
- [27] J. T. Klopogge, D. Wharton, L. Hickey, R. L. Frost, *Am. Mineral.* **2002**, *87*, 623–629.
- [28] M. B. Stevens, C. D. M. Trang, L. J. Enman, J. Deng, S. W. Boettcher, *J. Am. Chem. Soc.* **2017**, *139*, 11361–11364.
- [29] M. S. Burke, S. Zou, L. J. Enman, J. E. Kellon, C. A. Gabor, E. Pledger, S. W. Boettcher, *J. Phys. Chem. Lett.* **2015**, *6*, 3737–3742.
- [30] R. D. L. Smith, C. Pasquini, S. Loos, P. Chernev, K. Klingan, P. Kubella, M. R. Mohammadi, D. Gonzalez-Flores, H. Dau, *Nat. Commun.* **2017**, *8*, 2022.
- [31] B. M. Hunter, H. B. Gray, A. M. Müller, *Chem. Rev.* **2016**, *116*, 14120–14136.
- [32] R. Tsuchida, *Bull. Chem. Soc. Jpn.* **1938**, *13*, 388–400.
- [33] a) L. Fan, P. Zhang, B. Zhang, Q. Daniel, B. J. J. Timmer, F. Zhang, L. Sun, ACS Energy Lett. **2018**, *3*, 2865–2874; b) Y.-Y. Dong, D.-D. Ma, X.-T. Wu, Q.-L. Zhu, *Inorg. Chem. Front.* **2020**, *7*, 270–276.
- [34] Y. Ma, Z. Lu, S. Li, J. Wu, J. Wang, Y. Du, J. Sun, P. Xu, *ACS Appl. Mater. Interfaces* **2020**, *12*, 12668–12676.

Manuscript received: February 4, 2021

Accepted manuscript online: June 17, 2021

Version of record online: July 14, 2021